Accepted Manuscript

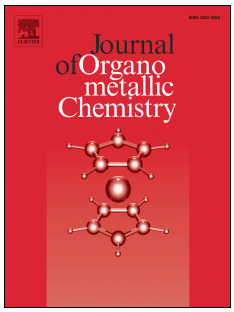

Synthesis and structure of arene ruthenium(II) benzhydrazone complexes: Antiproliferative activity, apoptosis induction and cell cycle analysis

Ramasamy Raj Kumar, Rengan Ramesh, Jan Grzegorz Małecki

PII: S0022-328X(18)30172-4

DOI: 10.1016/j.jorganchem.2018.03.013

Reference: JOM 20363

To appear in: *Journal of Organometallic Chemistry*

Received Date: 30 January 2018

Revised Date: 6 March 2018

Accepted Date: 10 March 2018

Please cite this article as: R. Raj Kumar, R. Ramesh, J.G. Małecki, Synthesis and structure of arene ruthenium(II) benzhydrazone complexes: Antiproliferative activity, apoptosis induction and cell cycle analysis, *Journal of Organometallic Chemistry* (2018), doi: 10.1016/j.jorganchem.2018.03.013.

Synthesis and structure of arene ruthenium(II) benzhydrazone complexes: Antiproliferative activity, apoptosis induction and cell cycle analysis

Ramasamy Raj Kumar [a], Rengan Ramesh[a,*], and Jan Grzegorz Małecki [b]

[a] Centre for Organometallic Chemistry, School of Chemistry, Bharathidasan University, Tiruchirappalli – 620 024, Tamil Nadu, India

[b] Department of crystallography, Institute of Chemistry, University of Silesia, 40-006 Katowice, Poland.

Keywords:

Bioorganometallic chemistry; Crystal structures; Lung cancer; Puckering amplitude; Apoptosis; Cell cycle analysis.

Corresponding author:

*E-mail: ramesh_bdu@yahoo.com; rrameshbdu@gmail.com Tel: +91-431-2407053; Fax: +91-431-2407045/2407020.

Abstract:

Synthesis of new half-sandwich ruthenium(II) complexes of the type [Ru(η^6-arene)(L)Cl] (arene = benzene or *p*-cymene; L = 1-pyrene-carboxaldehye benzhydrazone ligands) has been described. The synthesised complexes were completely characterised by elemental analysis and spectral (FT-IR, UV-vis, Emission, NMR and HRMS) methods. The isolated arene Ru(II) complexes are fluorescent in nature resulting the emission maxima observed in the visible region. The solid state molecular structures of the complexes 1, 2, 3 and 5 evidence that the ligands coordinate to ruthenium in a chelating κ^2 N, O- bidentate fashion, and shows the presence of typical pseudo-octahedral geometry. The potential of the complexes to act as anticancer agents are thoroughly screened on breast adenocarcinoma MCF-7, lung adenocarcinoma A549 and NIH-3T3 cell lines by *in vitro* experimental conditions. The anticancer activity of complex 4 is found to be remarkable towards A549 with high selectivity index and low IC_{50} values compared to cisplatin. The differences in biological activity of the complexes were explained on the basis of partition coefficient values and differences in the energy of ruthenium–chloride bonds. Further, AO/EB, Hoechst 33258 and flow cytometry analyses indicate that present ruthenium complexes cause cell death only *via* apoptosis mechanism. The DNA content in cell cycle distribution was analysed by flow cytometry which shows that complex 4 suppress the cell growth in A549 cells at sub G0/G1 phase region, indicative of apoptotic cells. This study outlines the preliminary steps towards understanding the mechanism of action with a new class of ruthenium-based chemotherapeutics.

1. Introduction

The milestone encounter of the antitumoral activities of cisplatin by Rosenberg in 1965 proclaim current field of medicinal inorganic chemistry depend on metallopharmaceuticals [1]. Till now, cisplatin and its congeners (carboplatin, nedaplatin, oxaliplatin, heptaplatin and lobaplatin) are some other most impressive chemotherapeutic agents in clinical use [2]. But, platinum-based drugs are some drawbacks such as intrinsic toxicity and extent of drug resistance persist the major challenges in their clinical application [3]. In the exploration for potential anticancer agents other than platimum, ruthenium compounds turned out to be the most encouraging ones [4]. Since ruthenium has been examined to be an enticing substitute to platinum, notably since most of the ruthenium compounds are less toxic and some

ruthenium compounds have been shown to be thoroughly judged for cancer cells [5, 6].

In recent years, Ru^{II}–arene compounds are highly regarded as potential anticancer agents [7,8]. The area of antitumoural and antimetastatic arene ruthenium complexes was instigated by Dyson and Sadler [9,10], The construction of arene-ruthenium based complexes as potential anticancer drugs due to their amphiphilic properties of the arene ruthenium unit, afforded by the combination of hydrophobic arene ligand and the hydrophilic metal centre [11]. One more interesting aspect is the hydrolysis of Ru–X bonds to give ruthenium-aqua species (aquation), although the arene–ruthenium bond is robust. The properties of the arene-ruthenium complexes depends on the π-acidic nature of η^6-arene moiety and substituent present in the ligand system. Further, Ru is stabilized in the +2 oxidation state [12,13]. Moreover, ruthenium complexes quite resemble with the ligand exchange kinetics of the platinum(II) in aqueous medium, which is also important force for antiproliferative activity.

Organometallic ruthenium(II)- arene 1, 2-diaminoethane (en) complexes of the type $[Ru(\eta^6\text{-arene})(en)X]^+$ (X = halide) have shown good cytotoxicity profiles [14]. RAPTA compounds of the common form $[Ru(\eta^6\text{-arene})(PTA)X_2]$ (PTA = 1,3,5-triaza-7-phosphaadamantane) were developed by the Dyson group [15] and their investigations afforded the two promising anticancer agents RM175 and RAPTA-C, which are currently at an advanced preclinical stage [16]. Arene-ruthenium(II) complexes with acylpyrazolones containing aliphatic groups in the acyl moiety along with their anticancer activity have been reported by Dyson *et al* [17]. Nathalie Wambang *et al* have explored the anticancer activity of new ruthenium complexes featuring indenoisoquinoline derivatives with a panel of cancer cell lines [18]. Ruthenium, rhodium and iridium complexes containing pyrene appended Schiff base ligands have been described [19,20]. In addition, Dyson group have reported the synthesis of new ruthenium half-sandwich complexes incorporating mixed ligands and their anticancer property [21].

Ligation of biologically active ligand systems to exploit synergistic effects as well as the high antitumour activity of the derived complexes is quite impressive to stimulate further research [22]. Aroylhydrazones are an paramount category of Schiff base ligands with interesting flexibility in bonding owing to presence of various coordination sites [23] and show remarkable biological activity [24]. Thus, hydrazone

analogues possessing an azomethine (-CONHN=CH-) group have been shown to exhibit antiproliferative activities and act as cytotoxic agents [25]. Design of hydrazone ligands is identical to present in biological framework, by typically making ligation *via* O and N donor atoms. Considering these facts, the design and synthesis of organometallic compounds decide an essential approach for increasing their pharmaceutical and biological activities. Pyrene and its analogues are known for their biologically activity with fluorescence properties and have been investigated as capable chemotherapeutic agents. The pyrene scaffold in conjugation with the metal centre or cyclometalated pyrene ring can further influence the biological properties of the system (Fig.1). A variety of mixed ligand complexes of copper, nickel, cobalt, palladium, platinum and ruthenium incorporating derivatives of hydrazone ligands have been reported [26-30], arene ruthenium(II) complexes encompassing benzhydrazone ligands and their biological properties are less viewed in the literature.

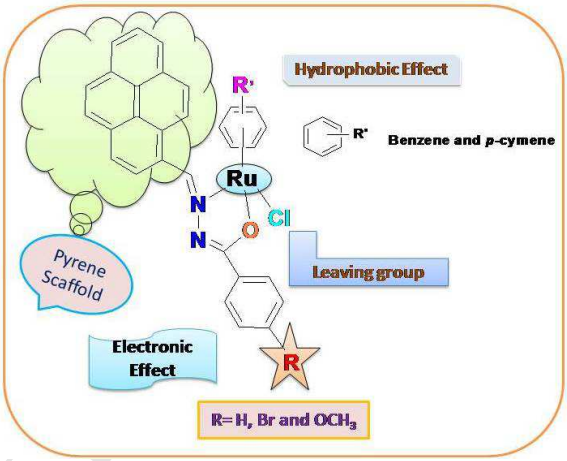

Fig.1 Design of Ru(II) arene 1-pyrenecarboxaldehyde benzhydrazone complexes.

We describe here, the synthesis and spectral studies of new arene ruthenium(II) benzhydrazone complexes with bidendate pyrene appended substituted benzhydrazone ligands along with chloride. Further, antiproliferative activity of the complexes was scrutinized towards various human cencer cell lines by MTT assay. The morphological changes and the investigations on their mode of action were illustrated by various bio-chemical assays. Apoptosis and cell cycle arrest were also carried out by flow cytometry.

2. Experimental section

2.1. Materials and physical measurements

Commercially available $RuCl_3.3H_2O$ was used as supplied from Loba chemie Pvt. Ltd. Pyrene-1-carboxaldehyde; substituted benzhydrazide analogue were purchased from sigma Aldrich and were used as received. All other chemicals were obtained from commercial source and were used as received. The solvents were distilled prior to use following the standard protocols. The arene dimer starting precausors $[(\eta^6\text{-}p\text{-cymene})RuCl_2]_2$ and $[(\eta^6\text{-benzene})RuCl_2]_2$ were prepared from reported literature procedure [31]. All other chemicals and reagents used for the biological studies were of high purity. Breast cancer cell line MCF-7, Lung cancer cell line A549 and Mouse embryo fibroblast cell line NIH 3T3 were received from National centre for cell Science (NCCS), Pune, India. 3-(4, 5-Dimethylthiazol-2-yl)-2, 5-diphenyltetrazolium bromide (MTT) were purchased from Sigma-Aldrich and used as received.

The microanalysis of (Carbon, Hydrogen and Nitrogen) was recorded by an analytical function testing Vario EL III CHNS elemental analyser. Melting points were noted with the aid of Boetius micro-heating table and are corrected. FT-IR spectra were recorded in Bruker ALPHA FT-IR spectrometer utilising KBr pellets. Electronic spectra in dichloromethane solution were reported with a CARY 300 Bio UV visible Varian spectrometer. Molar conductance studies were measured in DMF-H_2O solutions of the complexes (10^{-3}) using a model MK509 Digital TDS conductivity meter. Fluorescence spectral measurements were carried out using JASCO FP-5600 Spectrofluorimeter with 5 nm slit width. NMR spectra were taken on a Bruker 400 MHz instrument using tetramethylsilane (TMS) as an internal standard. ESI-HRMS spectra were employed in Thermo Fisher scientific with Scientific Exactive plus EMR model.

2.2. Preparation of benzhydrazone ligands

The mono basic bidendate benzhydrazone ligands were prepared by an ethanolic solution (10 mL) of 4-substituted benzhydrazide (1 mmol), an ethanolic (10 mL) solution of pyrene-1-carboxaldehyde (1 mmol) was added slowly. The reaction mixture was heated to reflux for 3 h, the solution concentrated to *ca* 5 mL and cooled to room temperature. The formed pale green solid was filtered, washed with cold methanol and dried in air. Yield: 80-88%.

Benzoic acid pyren-1-ylmethylene-hydrazide (L1): Colour: Pale-green; Yield: 80%; M.p.: 235 °C; Ana. Cal. For $C_{24}H_{16}N_2O$: C, 82.73; H, 4.62; N, 8.04. Found: C, 82.60; H, 4.55; N, 7.98. FT-IR (KBr, cm^{-1}) : 3213 s $\gamma_{(N-H)}$, 1637 s $\gamma_{(C=N)}$ + $\gamma_{(C=O).}$ ^{1}H NMR (400 MHz, DMSO-d_6): 12.0(s, 1H, NH), 9.5(s, 1H, CH=N), 8.8-8.7(d, J=9.2 Hz, 1H), 8.6-8.5(d, J=8 Hz, 1H), 8.3-8.0(m, 9H), 7.6-7.5(q, 3H) $L_{Aromatic-H}$ ppm. ^{13}C NMR (100 MHz, DMSO-d_6): 163.2(C=O), 146.5(C=N), 133.2, 133.9, 130.7, 130.0, 128.7, 128.6, 128.4, 127.5, 127.3, 126.8, 126.5, 126.0, 125.7, 125.2, 125.0, 124.0, 123.6 and 122.3($C_{Aromatic}$) ppm.

4-Bromo-benzoic acid pyren-1-ylmethylene-hydrazide (L2): Colour: Pale-green; Yield: 88%; M.p.: 242 °C; Ana. Cal. For $C_{24}H_{15}BrN_2O$: C, 67.46; H, 3.54; N, 6.56. Found: C, 67.28; H, 3.42; N, 6.48. FT-IR (KBr, cm^{-1}) : 3222 s $\gamma_{(N-H)}$, 1635 s $\gamma_{(C=N)}$ + $\gamma_{(C=O).}$ ^{1}H NMR (400 MHz, DMSO-d_6): 12.1(s, 1H, NH), 9.5(s, 1H, CH=N), 8.8(d, J=9.2 Hz, 1H), 8.5(d, J=8.4 Hz, 1H), 8.3(dd, J=7.6 Hz, 4H), 8.2(q, 2H), 8.1(t, J=15.2 Hz, 1H), 8.1-7.9(d, J=8.4Hz, 2H), 7.8(s, 2H) $L_{Aromatic-H}$ ppm. ^{13}C NMR (100 MHz, DMSO-d_6): 162.4(C=O), 146.9(C=N), 132.3, 132.0, 131.6, 130.7, 130.0, 129.6, 128.8, 128.6, 128.5, 127.3, 126.6, 126.1, 125.8, 125.7, 125.2, 125.1, 124.0, 123.6 and 122.3($C_{Aromatic}$) ppm.

4-Methoxy- benzoic acid pyren-1-ylmethylene-hydrazide (L3): Colour: Pale-green; Yield: 86%; M.p.: 250 °C; Ana. Cal. For $C_{25}H_{18}N_2O_2$: C, 79.34; H, 4.79; N, 7.40. Found: C, 79.25; H, 4.68; N, 7.45. FT-IR (KBr, cm^{-1}) : 3198 s $\gamma_{(N-H)}$, 1632 s $\gamma_{(C=N)}$ + $\gamma_{(C=O).}$ ^{1}H NMR (400 MHz, DMSO-d_6): 11.9(s, 1H, NH), 9.5(s, 1H, CH=N), 8.8(d, J=9.2 Hz, 1H), 8.5(d, J=7.6 Hz ,1H), 8.3(dd, J=8 Hz, 4H), 8.2(q, 2H), 8.1(d, J=7.6 Hz, 1H), 8.0-7.9(d, J=8.4 Hz, 2H), 7.1(d, J=8.8 Hz, 2H) $L_{Aromatic-H}$, 3.8(s, 3H, OCH_3) ppm. ^{13}C NMR (100 MHz, DMSO-d_6): 162.1(C=O), 145.9(C=N), 133.1, 131.8, 130.8, 130.1, 129.5, 128.8, 128.6, 128.5, 128.3, 127.3, 127.0, 126.5, 126.0, 125.7, 125.3, 125.2, 124.9, 124.1, 123.7, 122.3, 113.8($C_{Aromatic}$) and 55.4($C_{methoxy}$) ppm.

2.3. Synthesis of arene ruthenium(II) benzhydrazone complexes

The new complexes were prepared by the following general procedure: Benzene solution (20 mL) of $[(\eta^6\text{-arene})RuCl_2]_2$(arene = benzene or *p*-cymene) (0.05 mmol) was added the suitable pyrene fused substituted benzhydrazone ligand (0.1 mmol) and triethylamine (0.3 mL) as the base. The resulting reaction mixture was stirred at room temperature for 3 h and the reaction progress was monitored using TLC. At the end of the reaction, the solution was concentrated to *ca* 2 mL and addition of petroleum ether resulted in the formation of yellow and orange solid. The obtained complexes were recrystallized from DCM/pet.ether and dried under vacuum (Scheme 1).

$[Ru(\eta^6\text{-}C_6H_6)(Cl)(L1)]$ (1): Yellow solid. Yield: 77%; M.p.: 168°C; Ana. Cal. For $C_{30}H_{21}ClN_2ORu$: C, 64.11; H, 3.77; N, 4.98 % Found: C, 63.88; H, 3.69; N, 4.90 %. FT-IR (KBr, cm^{-1}): 1519 $\gamma_{(C=N-N=C)}$, 1437 $\gamma_{(N=C-O)}$, 1364 $\gamma_{(C-O)}$. UV–Vis (DCM, λ_{max}/nm (ε_{max}/dm^3 mol^{-1} cm^{-1}): 382 (6122), 280 (5808), 238 (13055). Molar conductance: 14.5 Scm^2mol^{-1}. ^{1}H NMR(400 MHz, $CDCl_3$): 9.7(s, 1H, HC=N), 9.1-9.0 (d, J=8 Hz, 1H), 8.2-8.0 (m,10H),7.3-7.1 (m,3H) $L_{Aromatic-H,}$ 5.0 (s, 6H, CH-benzene) ppm. ^{13}C NMR (100 MHz, $CDCl_3$): 174.9 (C-O),159.3 (C=N), ,132.7, 131.5, 131.2, 130.8, 130, 129.5, 129.2, 129.1, 128.9, 128, 127.3, 126.6, 126.5, 124.5, 124.3, 123.9, 122.8 ($C_{Aromatic}$), 84 ($C_{benzene}$) ppm. HR-ESI-MS(ACN) m/z: Found 563.0513 (calcd 563.0464).

$[Ru(\eta^6\text{- }C_6H_6)(Cl)(L2)]$ (2): Yellow solid. Yield: 75%; M.p.: 175°C; Ana. Cal. For $C_{30}H_{20}BrClN_2ORu$: C, 56.22; H, 3.15; N, 4.37 % Found: C, 55.95; H, 3.06; N, 4.28 %. FT-IR (KBr, cm^{-1}): 1519 $\gamma_{(C=N-N=C)}$, 1474 $\gamma_{(N=C-O)}$, 1384 $\gamma_{(C-O)}$. UV–Vis (DCM, λ_{max}/nm (ε_{max}/dm^3 mol^{-1} cm^{-1}): 386 (5043), 279 (4996), 240 (10872). Molar conductance: 13.2 Scm^2mol^{-1}. ^{1}H NMR(400 MHz, $CDCl_3$): 9.8 (s, 1H, HC=N), 9.0 (s, 1H), 8.4-8.0 (m,10H), 7.4(d, J=8Hz, 1H), 7.1 (s,1H $L_{Aromatic-H}$) , 5.0 (s, 6H, CH-benzene) ppm. NMR (100 MHz, $CDCl_3$): 174.0 (C-O), 159.4 (C=N), 132.7, 131.2, 131.1, 130.8, 130.7, 130.4, 129.9, 129.5, 129.2, 129.1, 127.3, 126.6, 126.5, 126.3, 125.2, 124.5, 124.3, 123.9, 122.7 ($C_{Aromatic}$), 84 ($C_{benzene}$) ppm. HR-ESI-MS(ACN) m/z: Found 640.9559 (calcd 640.9569).

$[Ru(\eta^6\text{-}C_6H_6)(Cl)(L3)]$ (3): Yellow solid. Yield: 72%; M.p.: 180 °C; Ana. Cal. For $C_{31}H_{23}ClN_2O_2Ru$: C, 62.89; H, 3.92; N, 4.73 % Found: C, 62.55; H, 3.80; N, 4.62 %.

FT-IR (KBr, cm^{-1}): 1505 $\gamma_{(C=N-N=C)}$, 1412 $\gamma_{(N=C-O)}$, 1366 $\gamma_{(C-O)}$. UV–Vis (DCM, λ_{max}/nm (ε_{max}/dm^3 mol^{-1} cm^{-1}): 385 (4449), 280 (4909), 239 (90095). Molar conductance: 12.4 Scm^2mol^{-1}. ^{1}H NMR(400 MHz, $CDCl_3$): 9.1 (s, 1H, HC=N), 8.5-8.4 (d, J=8.4 Hz, 1H), 8.3 (q,4H), 8.2-8.1 (q,4H), 8.1-8.0 (d, J=7.6 Hz, 1H), 6.9 (d, J=8.4Hz, 2H $L_{Aromatic-H}$), 3.8 (s,3H, OCH_3), 5.1 (s, 6H, CH-benzene) ppm. ^{13}C NMR (100 MHz, $CDCl_3$): 174.0 (C-O),159.4 (C=N), 132.6, 131.2, 130.8, 130.6, 129.9, 129.6, 129.4, 129, 128.6, 127.4, 126.6, 126.4, 126.2, 125.0, 124.4, 123.9, 122.9, 113.2 ($C_{Aromatic}$), 84($C_{benzene}$), 55.3($C_{methoxy}$) ppm. HR-ESI-MS(ACN) m/z: Found 593.0569 (calcd 593.0569).

[Ru(η^6-*p*-cymene)(Cl)(L1)] (4): Orange solid. Yield: 80%; M.p.: 178°C; Ana. Cal. For $C_{34}H_{29}ClN_2ORu$: C, 66.06; H, 4.73; N, 4.53 % Found: C, 65.81; H, 4.64; N, 4.56 %. FT-IR (KBr, cm^{-1}): 1584 $\gamma_{(C=N-N=C)}$, 1439 $\gamma_{(N=C-O)}$, 1382 $\gamma_{(C-O)}$. UV–Vis (DCM, λ_{max}/nm (ε_{max}/dm^3 mol^{-1} cm^{-1}): 390 (3737), 280 (3579), 238 (87492). Molar conductance: 19.1 Scm^2mol^{-1}. ^{1}H NMR(400 MHz, $CDCl_3$): 9.7 (s, 1H, HC=N), 9.2 (d, J=7.6 Hz, 1H), 9.1-8.0 (m,9H), 7.4-7.2 (q,4H $L_{Aromatic-H}$), 5.4 (d, J=6 Hz, 1H, cymene Ar-H), 5.1 (d, J=6 Hz, 1H, cymene Ar-H), 4.5 (d, J=5.6 Hz, 1H, cymene Ar-H), 3.7 (d, J=5.2 Hz, 1H, cymene Ar-H), 2.5 (m, 1H, CH of *p*-cymene), 2.1 (s, 3H, CH_3 of *p*-cymene), 1.0 (d, J=24.4 Hz, J=6.8 Hz, 6H, $2CH_3$ of *p*-cymene) ppm. ^{13}C NMR (100 MHz, $CDCl_3$): 174.9(C-O), 158.4 (C=N), 132.5, 132.1, 131.2, 130.7, 130.5, 129.8, 129.7, 129.3, 129, 128.9, 128.8, 127.9, 127.8, 127.4, 126.6, 126.4, 126.2, 125.9, 124.5, 124.4, 123.9, 122.7($C_{Aromatic}$ and $CH_{Aromatic}$). 102.1 and 100.2 ($C_{quternary\ of\ cymene}$), 85.8-80.4 ($C_{aromatic\ of\ cymene}$), 30.8 ($CH_{\ of\ P\text{-}cymene}$), 22.3, 22.1 ($2CH_{3\ of\ cymene}$), 18.9 ($CH_{3\ of\ cymene}$) ppm. HR-ESI-MS(ACN) m/z: Found 619.1083 (calcd 619.1090).

[Ru(η^6-*p*-cymene)(Cl)(L2)] (5): Orange solid. Yield: 82%; M.p.: 188°C; Ana. Cal. For $C_{34}H_{28}BrClN_2ORu$: C, 58.59; H, 4.05; N, 4.02 % Found: C, 58.30; H, 3.79; N, 3.93 %. FT-IR (KBr, cm^{-1}): 1522 $\gamma_{(C=N-N=C)}$, 1481 $\gamma_{(N=C-O)}$, 1377 $\gamma_{(C-O)}$. UV–Vis (DCM, λ_{max}/nm (ε_{max}/dm^3 mol^{-1} cm^{-1}): 390 (3517), 280 (3616), 239(81594). Molar conductance: 15.8 Scm^2mol^{-1}. ^{1}H NMR(400 MHz, $CDCl_3$): 9.7 (s, 1H, HC=N), 9.1 (d, J=8 Hz, 1H), 8.2-8.0 (m,5H), 8.4-8.3 (m,5H), 7.5 (d, J=8.4 Hz, 2H $L_{Aromatic-H}$), 5.4 (d, J=6 Hz, 1H, cymene Ar-H), 5.1 (d, J=6 Hz, 1H, cymene Ar-H), 4.5 (d, J=5.6 Hz, 1H, cymene Ar-H), 3.7 (d, J=5.6 Hz, 1H, cymene Ar-H), 2.5 (m, 1H, CH of *p*-cymene), 2.1 (s, 3H, CH_3 of *p*-cymene), 1.0 (d, J=24.4 Hz, J=7.2 Hz, 6H, $2CH_3$ of *p*-cymene)

ppm. ^{13}C NMR (100 MHz, $CDCl_3$): 172.9 (C-O), 157.8 (C=N), 131.6, 130.2, 130, 129.7, 129.5, 129.4, 128.8, 128.6, 128.5, 128.4, 127.9, 126.3, 125.6, 125.4, 125.2, 124, 123.5, 123.4, 122.9, 121.6 ($C_{Aromatic}$ and $CH_{Aromatic}$). 101.2 and 99.3($C_{quternary\ of\ cymene}$), 84.7-80.4($C_{aromatic\ of\ cymene}$), 29.8($CH_{\ of\ cymene}$), 21.2, 21.1($2CH_{3\ of\ cymene}$), 17.9($CH_{3\ of\ cymene}$) ppm. HR-ESI-MS(ACN) m/z: Found 697.0178 (calcd 697.0195).

[Ru(η^6-*p*-cymene)(Cl)(L3)] (6): Orange solid. Yield: 78%; M.p.:185°C; Ana. Cal. For $C_{35}H_{31}ClN_2O_2Ru$: C, 64.86; H, 4.82; N, 4.32 % Found: C, 64.62; H, 4.60; N, 4.20 %. FT-IR (KBr, cm^{-1}): 1510 $\gamma_{(C=N-N=C)}$, 1435 $\gamma_{(N=C-O)}$, 1366 $\gamma_{(C-O)}$. UV–Vis (DCM, λ_{max}/nm (ε_{max}/dm^3 mol^{-1} cm^{-1}): 388 (4435), 278 (4401), 238 (95583). Molar conductance: 16.9 Scm^2mol^{-1}. ^{1}H NMR(400 MHz, $CDCl_3$): 9.7 (s, 1H, HC=N), 9.1 (d, J=8 Hz, 1H), 8.4 (d, J=9.2 Hz, 1H), 8.3-8.0 (m,8H), 7.2(s,1H), 6.9-6.8 (d, J=8.4 Hz, 2H $L_{Aromatic-H}$), 5.4 (d, J=6 Hz, 1H, cymene Ar-H), 5.1 (d, J=6 Hz, 1H, cymene Ar-H), 4.5 (d, J=5.6 Hz, 1H, cymene Ar-H), 3.8 (s,3H, OCH_3), 3.7 (d, J=5.6 Hz, 1H, cymene Ar-H), 2.5 (m, 1H, CH of *p*-cymene), 2.1 (s, 3H, CH_3 of *p*-cymene), 1.0 (d, J=24.4 Hz, J=6.8 Hz, 6H, $2CH_3$ of *p*-cymene) ppm. ^{13}C NMR (100 MHz, $CDCl_3$): 174.7 (C-O), 157.5 (C=N), 132.4, 131.2, 130.8, 130.6, 129.9, 129.8, 129.3, 128.8, 128.3, 127.4, 126.5, 126.3, 126.1, 124.6, 124.5, 124.4, 123.9, 122.8, 113.1 ($C_{Aromatic}$ and $CH_{Aromatic}$). 102.0 and 100.1($C_{quternary\ of\ cymene}$), 85.8-80.3($C_{aromatic\ of\ cymene}$), 55.3($C_{methoxy}$), 30.8($CH_{\ of\ cymene}$), 22.3, 22.1($2CH_{3\ of\ cymene}$), 18.9($CH_{3\ of\ cymene}$) ppm. HR-ESI-MS(ACN) m/z: Found 649.1188 (calcd 649.1195).

2.4. X-ray crystallography

Single crystal of the **1**, **2, 3** and **5** complexes convenient for X–ray diffraction studies were grown by slow evaporation of dichloromethane-methanol mixture at room temperature. A single crystal of suitable size was mounted in turn on an Gemini A Ultra Oxford Diffraction automatic diffractometer equipped with a CCD detector, and used for data collection. X-ray intensity data were collected with graphite monochromated Mo-Kα radiation (λ = 0.71073 Å) at a temperature of 295(2) K, with the ω scan mode. Ewald sphere reflections were collected up to 2θ = 50.101. Lorentz, polarization and empirical absorption corrections using spherical harmonics implemented in the SCALE3, ABSPACK scaling algorithm. The Olex2 and SHELXS, SHELXL programs were applied for all the calculations [32,33].

2.5. Stability studies

The stabilities of the complexes in solutions were checked by registering the UV-Vis spectra of then in the DMSO/aqueous phosphate buffer solutions (1×10^{-3} M). The hydrolysis profiles were recorded by monitoring the spectra over 48h at distinct time intervals.

2.6. Cell culture and inhibition of cell growth

The cell lines were cultured as a monolayer in RPMI-1640 medium (Biochrom AG, Berlin, Germany), supplemented with 10% fetal bovine serum (Sigma-Aldrich, St. Louis, MO, USA) and with 100 UmL^{-1} penicillin and 100 μg mL^{-1} streptomycin as antibiotics (Himedia, Mumbai, India). All the cells were grown at 37°C under a 5% CO_2 atmosphere. The IC_{50} values, which are the concentrations of the tested complexes that inhibit 50% of cell growth, were calculated using MTT assay. Cells were plated in their growth medium at a density of 5000 cells per well in 96 flat-bottomed well plates. After plating, complexes 1-6 were added at different concentrations (0.1-100 μM for 48 h, with a final volume in the well of 250 μL) for 48 h to investigate the dose-dependent cytotoxic activity. To each well, 20 μL of 5 mg mL^{-1} MTT in phosphate buffer (PBS) was added. The plates were wrapped with aluminium foil and incubated for 4 h at 37°C. The purple formazan product was dissolved by addition of 100 μL of 100% DMSO to each well. The quantity of formazan formed gave a measure of the number of viable cells. MCF-7, A549 and NIH 3T3 were used for the MTT assay. The absorbance was monitored at 570 nm (measurement) and 630 nm (reference) using a 96 well plate reader (Bio-Rad, Hercules, CA, USA). Data were collected for four replicates each and used to find the respective means. The percentage of inhibition (IC_{50} value) was calculated, from this data, using the formula: Percentage inhibition = 100 x {Mean OD of untreated cells (control) - Mean OD of treated cells}/{Mean OD of untreated cells (control)}.

2.7. Partition coefficients determination

Partition coefficient (P) between octanol–water phase of the synthesised arene ruthenium(II) complexes were measured by using “Shake flask” method [34]. The Partition coefficient P is the ratio between the concentrations of a compound dissolved in the two immiscible solvents, usually n-octanol and water. Complexes were dissolved in a mixture of water and n-octanol followed by shaking for 1 hour. The mixture was allowed to settle over a time of 30 minutes and the resulting two phases

were collected individually without cross contamination of one solvent layer into another. Finally, the concentration of the complexes in each phase was analysed by UV-vis absorption spectroscopy at room temperature. Partition coefficients for **1-6** were calculated from the following equation logP = log $[(1\text{-}6)_{oct}/(1\text{-}6)_{aq}]$. The results are given as the mean values taken from three independent experiments.

2.8. AO/EB dual staining experiment

The A549 cells were treated with complex **4** at IC_{50} concentration and incubated for 48 h in CO_2 incubator at 37°C. The cells were removed by trypsination and collected by centrifugation including the non-adherent cells. The cell pellets were resuspended in medium and cell suspensions (25 µL) were transferred to glass slides. Dual fluorescent staining solution, with 25 µL of AO and EB solution(1 part of 100 µg mL^{-1} AO and 1 part of µg mL^{-1} EB in PBS) and examined at 20x magnifications in a laser scanning confocal microscope LSM 710 (Carl Zeiss, Germany) using an UV filter (450–490 nm).

2.9. Hoechst 33258 staining method

Hoechst 33258 staining was performed using a method described earlier but with minor modifications. A549 cells 5×10^5 were treated with IC_{50} concentrations of complex **4** for 24 h in a 6-well culture plate and fixed with 4% paraformaldehyde followed by permeabilization with 0.1% Triton X-100. Cells were then stained with 50 $\mu g.mL^{-1}$ Hoechst 33258 for 30 min at room temperature. The cells undergoing apoptosis, represented by the morphological changes of apoptotic nuclei, were observed and imaged using an epifluorescence microscope (Carl Zeiss, Germany).

2.10. Flow cytometry/Annexin V-PI staining

Annexin FITC staining was determined using Annexin V-FITC staining kit SC 4252 (Santa Cruz) as per the manufacture's instruction. Briefly A549 cells after indicated treatments were trypsinised and washed with 1x Annexin binding buffer followed by staining with Annexin V FITC and PI. The cells were incubated in staining buffer for 15 minutes at 37°C. The stained cells were washed in binding buffer and analysed using flow cytometer FACS AriaII. (Becton Dickinson). The FITC was excited with 488 nm laser and PI using 562 nm laser lines. The results were ascertained by using DIVA software and percentage positive cells were carefully calculated.

2.11. Cell cycle analysis

Briefly A549 cells after indicated treatments were trypsinised and washed with PBS followed by fixation of cells in ethanol for 1 hour at 4°C. The fixed cells were then subjected to RNase treatment (20ug/mL) for 1 hour at 37°C, later stained with PI (40-50ug/mL) for 10 minutes at 37°C. The stained cells were analyzed using flow cytometer FACS AriaII. (Becton Dickinson). The PI was excited with 562 nm laser line.

2.12. DFT calculations

The bonding interactions between the Cl ligand with ruthenium complex fragments have been analyzed by means of the energy decomposition analysis, based on the work of Morokuma, and the extended transition state (ETS) partitioning scheme of Ziegler have been carried out using the ADF program (Release 2008) at the level of B3LYP/TZP[35,36]. The binding energy of each compound was calculated as the difference between the energy of the geometry optimized coordination compounds and the energies of the optimized Cl^- ligand anion and the $[(benzene/p\text{-}cymene)RuL]^+$ fragment. The general theoretical background on the bond energy decomposition scheme has been reviewed [37-39].

3. Results and discussion

3.1. Synthesis and spectral characterization of arene Ru(II) benzhydrazone complexes

Mono-basic bidendate hydrazone ligand derivatives were quickly prepared by condensation reactions of equimolar amounts of 1-pyrene carboxaldehyde with substituted benzhydrazides. The reactions of 2 ligand equivalent (L1-L3) with 1 equivalent of ruthenium(II) arene dimer $[Ru(\eta^6\text{-arene})Cl_2]_2$ (arene-benzene or p-cymene) in the presence of NEt_3 offer complexes with general formula of $[Ru(\eta^6\text{-arene})(L)Cl]$ (arene= benzene or *p*-cymene (Scheme 1) in good yields. The synthesised complexes are stable in air and highly soluble with common organic solvents.

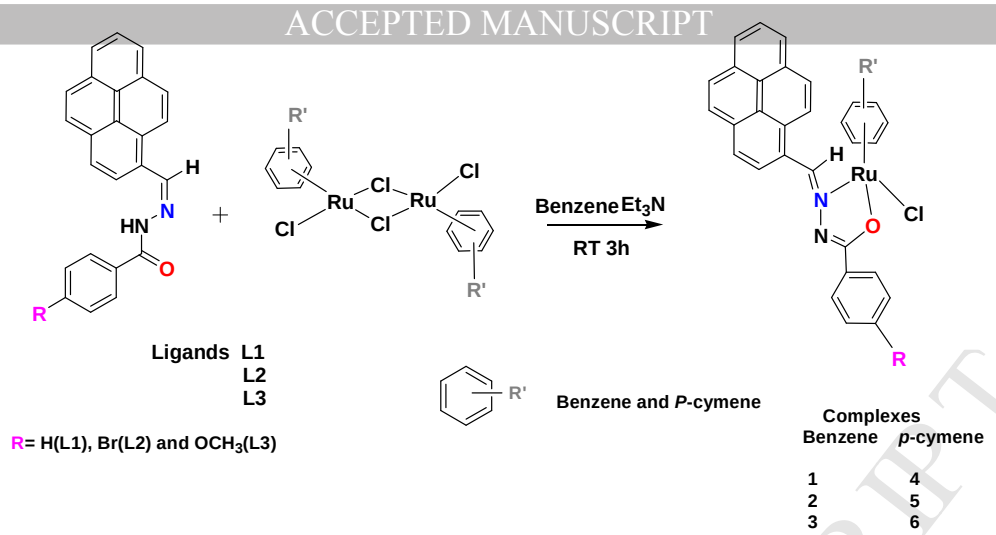

Scheme1. Synthesis of arene ruthenium(II) benzhydrazone complexes.

FT-IR spectra of the free ligands and the respective arene ruthenium(II) complexes provided useful information about the metal–ligand coordination modes. The hydrazone ligands displayed a medium to strong bands in the region of 3222- 3198 cm^{-1} which represents the N-H functional group. The ligands also showed two different absorptions $\gamma_{C=N}$ and $\gamma_{C=O}$ in the range of 1505-1584 cm^{-1} and 1632-1637cm^{-1} respectively. The existence of tautomerization and coordination *via* imidolate oxygen were observed based on the disappearance of γ_{N-H} and $\gamma_{C=O}$ bands in all of the complexes. Further, the appearance of the band at 1364–1384 cm^{-1} proves the coordination of imidolate oxygen to ruthenium(II) ion [40]. A new band in the region of 1505- 1584 cm^{-1} illustrates the azomethine nitrogen coordinated to metal.

Electronic spectra of the complexes 1-6 were recorded in dichloromethane solution and the spectra are depicted in Fig. S1(ESI†). The complexes display three absorptions bands in the region of 238–390 nm. The high intense bands in the region of 238–280 nm correspond to ligand-centered transitions and have been labelled as π-π* and n-π* transitions with possible contributions from benzhydrazone ligand moiety. The medium intense band in the range of 382-390 nm observed in all of the complexes is due to MLCT transitions similar to other octahedral ruthenium(II) arene complexes [41]. The emission measurements of all the complexes were carried out in CH_2Cl_2 solutions at ambient temperature. The emission maxima of the ruthenium complexes have accomplished a positive move in the magnitude of 110-116 nm and fall in the range of 470-476 nm.

NMR spectroscopy techniques were used to find out the bonding arrangement between the ligand and metal ion. The spectra of the ligands and the complexes were obtained in DMSO-d_6 and $CDCl_3$ solutions and are depicted in Fig. S2 and S4(ESI†). The aromatic protons of the coordinated ligands are appeared as multiplets in the region of 6.8-9.2 ppm. Azomethine protons appeared as singlets in the region of 9.8-9.1 ppm in spectra of all the complexes. These are marginally downfield shifted compared with the free ligand, implying coordination of azomethine nitrogen to ruthenium. In the complexes, the singlet signal of -NH proton of the free ligand is absent indicating enolisation and ligation of the imidolate oxygen to the Ru(II) ion. In the complexes, the *p*-cymene protons appear as four sets of doublets in the range of 3.7–5.4 ppm and methoxy protons are detected as a singlet for complexes **3** and **6** at 3.8 ppm. The isopropyl CH proton shows a septet in the range of 2.4–2.6 ppm and methyl protons come out as a singlet at 2.1 ppm. Additionally, the isopropyl protons of the *p*-cymene appear as pair of doublets in the range of 1.0–1.1 ppm. Coordinated benzene protons in the case of **1-3** complexes displayed singlet signals at 5.0-5.1 ppm. The ^{13}C NMR spectra of all ligands and complexes were produced resonance in the expected region and the spectra are given in Fig. S3 and S5 (ESI†). The signals of the aromatic carbons showed at 113-132 ppm. Also, the complexes (157-159 ppm) show a down field shift of the imine carbon (–C=N–) with respect to the free ligands (145-146 ppm) which was assigned to ligation of the imine nitrogen to the Ru centre. Further, the signal designated to the imidolate carbon (–NH–C=O) shifts from 162-163 ppm in the free ligand into 172-174 ppm in the Ru(II) complexes, as a result of reduced bond order (–N=C–O) at the time of coordination. The signals noted at 84.0 ppm and 17.9-18.9, 101.2-102.1 ppm evidenced the presence of benzene (**1-3**) and *p*-cymene (**4-6**) of the ruthenium(II) arene complexes respectively.

The composition and fragmentation pattern of the complexes were also acquired from high resolution mass spectral studies. High resolution mass spectrometric measurements were performed under positive ion ESI mode using acetonitrile as the solvent. The HRMS spectra of the complexes display peaks at m/z 563.0513 [1, $M+H]^+$, 640.9559 [2, $M+H]^+$, 593.0569 [3, $M+H]^+$, 619.1083 [4, $M+H]^+$, 697.0178 [5, $M+H]^+$, and 649.1188 [6, $M+H]^+$, respectively. The results from mass spectral analyses are in close agreement with the molecular formulae proposed for all the complexes.

3.2. X-ray crystallographic studies

As side of the structural characterization, the solid state crystal structures of four complexes, i.e. **1, 2, 3** and **5** have been derived using X-ray diffraction analysis. Slow evaporation of dichloromethane-methanol solutions of the complexes generated single crystals of suitable size for diffraction. The crystallographic data and structural refinement parameters are given in Table 1 while the selected bond lengths and angles are gathered in Table 2. The ORTEP diagrams of the complexes are shown in Fig. 2-5. The complex **1** crystallized in the triclinic space group *P*-1 whereas the complexes **2, 3** and **5** in the $P2_1/c$ monoclinic space group. The structure of complex **1** shows exactly that the ligand behaves as a bidentate donor to ruthenium ions *via* the azomethine nitrogen and imidolate oxygen leftover to one chloride and one arene group. The geometry around the ruthenium atom is the classic three-legged piano-stool arrangement with pseudo-octahedral geometry and display features similar to other reported arene ruthenium(II) complexes. In this complex, the arene ring forms the seat of the piano-stool, whereas the benzhydrazone and a chloro group pattern the three legs. Hence, the metal ion is situated in a (η^6-arene) NOCl coordination environment. The benzhydrazone ligand coordinates to Ru centre at N and O donor atoms assemble the five membered chelate ring with the corresponding bite angles of 76.51(8)° O(1)–Ru(1)–N(1) and 86.48(7)° N(1)–Ru(1)–Cl(1). The bond distance between Ru(1)–N(1) and Ru(1)–O(1) are 2.4098(9) Å and 2.0594(19) Å respectively. The bond length of ruthenium and chloride is 2.4172(16) Å and the distance is very similar to other reported for arene ruthenium(II) complexes [42]. The average Ru–C distance in the arene moiety is 2.176(7) Å. It has been observed that complexes **2, 3** and **5** also endorses a similar geometrical environment as in **1** with small variations in the bond angles and distances.

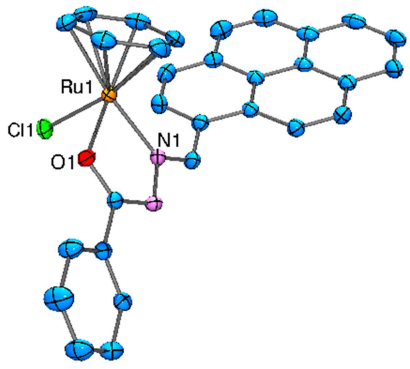

Fig.2. ORTEP drawing of [Ru(η^6-C_6H_6)(Cl)(L1)] (**1**), at the 30% probability level. The solvent molecule and hydrogen atoms are omitted for clarity.

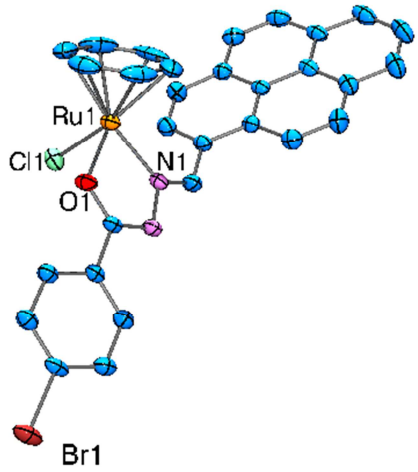

Fig.3. ORTEP drawing of [Ru(η^6-C_6H_6)(Cl)(L2)] (**2**), at the 30% probability level. The solvent molecule and hydrogen atoms are omitted for clarity.

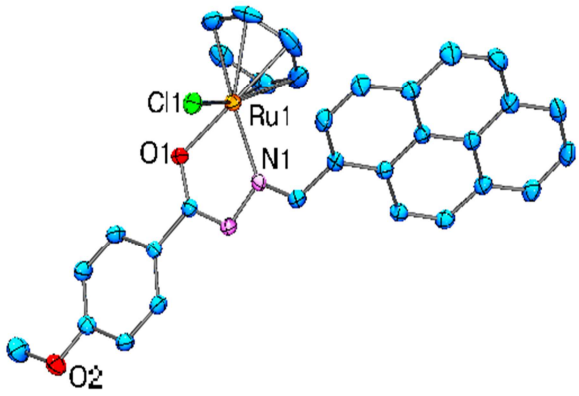

Fig. 4. ORTEP drawing of [Ru(η^6-C_6H_6)(Cl)(L3)] (**3**), at the 30% probability level.

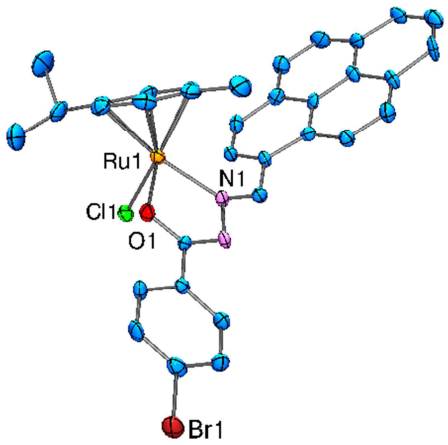

Fig. 5. ORTEP drawing of [Ru(η^6-*p*-cymene)(Cl)(L2)] (**5**), at the 30% probability level.

Table 1: Crystal data and structure refinement parameters for complexes 1, 2, 3 and 5

	Complex **1**.CH_2Cl_2	Complex **2**.CH_3OH	Complex **3**	Complex **5**
Empirical formula	$C_{30}H_{21}ClN_2ORu$	$C_{30}H_{20}ClBrN_2ORu$	$C_{31}H_{23}ClN_2O_2Ru$	$C_{34}H_{28}BrClN_2ORu$
Formula weight	562	640.9	592.03	697.01
Colour	Brown	Red	Red	Red
CCDC number	1543439	1522090	1522136	1517739
Temperature (K)	295(2)	295(2)	295(2)	295(2)
Wavelength (Å)	0.71073	0.71073	0.71073	0.71073
Crystal system	Triclinic	Monoclinic	Triclinic	Monoclinic
Space group	*P-1*	*P*2(1)/C	*P-1*	*P*2(1)/C
a (Å)	10.0505(4)	14.3341(7)	10.0980(6)	19.4207(10)
b (Å)	11.5442(5)	7.6374(4)	10.7546(6)	13.8092(8)
c (Å)	12.9889(5)	24.2106(15)	13.0345(8)	22.4894(15)
α (°)	99.129(3)	90	106.810(5)	90
β (°)	106.565(3)	100.206(6)	105.023(5)	105.284(6)
γ (°)	103.828(4)	90	101.047(5)	90
Volume ($Å^3$)	1360.34(10)	2608.5(3)	1253.16(14)	5818.0(6)
Z	2	4	2	8
$\rho_{calcd.}$ ($Mg\ m^{-3}$)	1.579	1.714	1.569	1.591
μ (mm^{-1})	0.899	2.269	0.765	2.035
F(000)	652	1344	600	2800
Crystal size (mm)	0.03 x 0.16 x 0.33	0.08 x 0.09 x 0.34	0.03 x 0.12 x 0.19	0.06 x 0.12 x 0.47
Theta range (°)	3.91 to 27.17	3.42 to 29.50	3.81 to 27.98	3.62 to 27.60
Limiting indices	$-12 \le h \le 13$, $-15 \le k \le 11$, $-16 \le l \le 15$	$-12 \le h \le 19$, $-7 \le k \le 10$, $-33 \le l \le 31$	$-10 \le h \le 13$, $-13 \le k \le 14$, $-17 \le l \le 16$	$-24 \le h \le 26$, $-15 \le k \le 19$, $-31 \le l \le 21$
Reflections collected/unique	6365/4852	6221/4218	5855/4415	13874/7997
Data/restraints/parameters	6365/0/343	6221/0/333	5855/0/335	13874/0/727
Final *R* indices [$I>2\sigma(I)$]	R_1 =0.0698, wR_2 = 0.0835	R_1 =0.0457, wR_2 = 0.0832	R_1 =0.0719, wR_2 = 0.1100	R_1 =0.0988 wR_2 = 0.2198
R indices (all data)	R_1 =0.0447, wR_2 = 0.0977	R_1 =0.0839, wR_2 = 0.0966	R_1 =0.04999, wR_2 = 0.1208	R_1 =0.1653, wR_2 = 0.2486
Largest diff. Peak and hole	0.51 and -0.67 e. $Å^{-3}$	0.439 and -0.543 e. $Å^{-3}$	1.23 and -0.75 e. $Å^{-3}$	1.556 and -1.240 e. $Å^{-3}$

Table 2: Selected bond lengths (Å) and bond angles (°) for ligand and complexes 1,2,3 and 5.

Complex **1**	Complex **2**	Complex **3**	Complex **5**
Bond Length (Å)			
Ru1N1 2.4098(9)	Ru1N1 2.084(5)	Ru1N1 2.091(3)	Ru1N1 2.084(5)
Ru1O1 2.0594(19)	Ru1O1 2.055(3)	Ru1O1 2.062(2)	Ru1O1 2.055(3)
Ru1 Cl1 2.4172(16)	Ru1 Cl1 2.4172(16)	Ru1 Cl1 2.4014(10)	Ru1 Cl1 2.4172(16)
N1 N2 1.411(3)	N1 N2 1.417(5)	N1 N2 1.404(4)	N1 N2 1.417(5)
O1 C1 1.292(4)	O1 C1 1.289(6)	O1 C1 1.294(4)	O1 C1 1.289(6)
N2 C1 1.302(4)	N2 C1 1.316(7)	N2 C1 1.306(4)	N2 C1 1.316(7)
Bond Angle (°)			
O1 Ru1 N1 76.51(8)	O1 Ru1 N1 76.30(10)	O1 Ru1 N1 76.30(9)	O1 Ru1 N1 76.4(3)
O1 Ru1 Cl1 85.21(7)	O1 Ru1 Cl1 83.40(8)	O1 Ru1 Cl1 86.25(8)	O1 Ru1 Cl1 85.2(2)
C1 O1 Ru1 112.75(17)	C1 O1 Ru1 113.5(2)	C1 O1 Ru1 113.2(2)	C1 O1 Ru1 113.4(6)
N2 N1 Ru1 113.82(17)	N2 N1 Ru1 114.9(2)	N2 N1 Ru1 114.38(18)	N2 N1 Ru1 113.7(6)
C1 N2 N1 111.2(2)	C1 N2 N1 110.0(3)	C1 N2 N1 115.5(3)	C1 N2 N1 112.2(8)
N1 Ru1 Cl1 86.48(7)	N1 Ru1 Cl1 83.77(8)	N1 Ru1 Cl1 84.29(8)	N1 Ru1 Cl1 84.7(2)

3.3. Stability studies

The stability of ruthenium complexes in aqueous solution was measured over various time intervals using a UV-visible spectrophotometer. The stock solution of the complexes in DMSO was prepared and diluted using aqueous phosphate buffer solution pH 7.4, and finally made into 1×10^{-3} M concentration. At different time intervals, the spectra of the complexes were recorded at room temperature and are shown in Fig. S6 (ESI†). From the spectral diagrams, we did not identify any changes in the spectral patterns of the complexes over 48 h intervals. Further, the conductivity measurements for the complexes 1-6 were measured in DMSO-H_2O (10^{-3} M) solutions at room temperature. The obtained molar conductivities values of the complexes indicate the hydrolysis takes place in solution. Hence, it is concluded that the activity of the complexes is dependent of their ability to exchange chlorine ligand into water under cellular conditions.

3.4. *In vitro* anticancer activity

Anticancer activity of the arene ruthenium complexes were carried out against MCF-7 and A549 along with NIH 3T3 by measuring the cell viability analysis by using colorimetric assay and cisplatin was entered as a standard drug. The capacity of the ruthenium complexes to capture the propagation of cancer cells was investigated after an incubation time of 48 h and are shown in Fig. S7 an S8 (ESI†). Cytotoxicity results were analysed by the aid of cell viability curves and expressed with values in the concentrations of 0.1-100 μM. The concentrations of the tested complexes that inhibit 50% of cell growth represented as IC_{50} values are noted. Results to be recognized that the precursor and the ligand did not show any inhibition of the cell growth even up to 100 μM (Table 3).

The complexes **1–6** possess good cytotoxicity profiles over the ligands which may be due to form strong adducts with DNA as a result of processes such as direct coordination, intercalation or H-bonding to DNA. The hydrolysis reaction or the exchange of a halogen on water plays an important role in the processes. The geometrical parameters influence the Ru–Cl bonding stability and the biological activity of these complexes may be related to formation of corresponding aqua species. In the studied compounds the angle between planes of the phenyl coordinated to Ru atom and pyrene moiety in the complexes (**2**, **3**, **5** and **6**) is high based on puckering amplitude. Further, the angle between planes of phenyl group coordinated to Ru atom and pyrene is smaller in the case of **1** and **4**, which affects the ruthenium-chloride bond strength. The geometrical parameters were calculated on the basis of structural data obtained from X-ray measurements for monocrystals. The parameters will change in the solutions and therefore we calculate the bonding energies between the chloride ligand (Cl^-) and ruthenium core ($[(arene)RuL]^+$) for all studied complexes. From the data collected in Table S1 (ESI†) in the case of complex **4** the exchange of chloride ligand on water occurs most easily. Overall, the complexes containing *p*-cymene group show higher potency than those with a benzene group in complexes **1-3**, which may be due to the stronger hydrophobic interactions between metal center and the targeted biomolecules. Particularly, complex **4** shows high cytotoxicity with low IC_{50} value of 11.9 ±0.7 μM towards A549 cell lines. The selectivity index (SI) for all of the complexes is expressed as the IC_{50} of the pure compound in a normal cell line/the IC_{50} of the pure compound in a cancer cell line.

The calculated selectivity index for complexes **1-6** are 6.7, 4.6, 5.0, 12.1, 5.7, 6.1 and 7.9, 4.8, 6.1, 18.9, 5.1, 7.0 against MCF-7 and A549 cell lines, respectively. It is to note that complex **4** exhibits strong selectivity towards the tested cancer cells. Altogether our findings suggest that the high lipophilic polycyclic aromatic compounds i.e. pyrene motif used for the systematic examination of selective membarane interactions with malignant cells as a main role in cell killing and the observed biological activity. Furthermore, the IC_{50} values obtained for the complexes are enough lower than reported for other Ru(II) arene complexes [20,43,44]. The IC_{50} value specified for the complexes against NIH-3T3 (normal cell line) is found to be above 220 μM, which confirms that the complexes are very specific to cancer cells and even less toxic than cisplatin. These supportive findings encouraged us to extend the studies, that the selectivity between cancer and normal cells, and may be suggested as suitable candidates for chemotherapeutic drugs.

Table 3. Cytotoxicity (IC_{50}, μM) of the ligand, complexes **1-6** (n. e.: no effect) and Calculated selectivity index (SI).

	IC_{50} (μM) (mean±SD)				
Complexes	MCF-7	SI	A549	SI	NIH-3T3
1	35.7±1.2	6.7	30.3±1.2	7.9	240.1±0.4
2	50.5±0.5	4.6	48.4±2.8	4.8	235.5±1.2
3	48.4±1.2	5.0	40.1±0.5	6.1	245.1±0.8
4	18.5±0.6	12.1	11.9±0.7	18.9	225.3±0.5
5	40.2±0.3	5.7	45.0±1.1	5.1	230.5±2.3
6	35.8±1.5	6.1	31.4±3.5	7.0	220.1±1.4
L1	>100	---	n.e	---	n.e
L2	n.e	---	n.e	---	n.e
L3	n.e	---	108.1±0.6	---	n.e
Cisplatin	12.6±0.8	13.8	18.5±1.4	9.4	175.1±1.8

3.5. Partition coefficients determination

One more important aspect that has been studied for anticancer activity of the complexes is their lipophilicity. This was explored by the partition coefficient, P as an index of molecular lipophilicity of a drug, which is linked to its capacity to cross cell membranes by the aid of static diffusion (n-octanol models the lipid bilayers of cell

membranes and water produce the fluid in and out of cells [45,46]. -0.67, -1.45, -1.34, -0.37, -1.36 and -1.28 are the calculated log P values for complexes 1-6 respectively. It has been observed that complex **4** with *p*-cymene moiety shows higher activity than the rest of the complexes.

3.6. AO/EB and Hoechst 33258 staining assays

To investigate the apoptosis inducing properties of the complexes, fluorescence acridine orange/ethidium bromide staining was performed and the representative images of control and treated cells are shown in Figure 6. The gross cytological features like cytoplasmic shrinkage, membrane blebbing and nuclear condensation, which is the typical characteristic of cells undergoing apoptosis. A549 cells are stained by AO/EB, following 48 h incubation with complex **4**. The control cells are dense and showed steady green fluorescence uniformly dispersed chromatin in the nucleus of live cells. On extended treatment of cells for 48 h at the IC_{50} concentration of the complex **4**, congregated chromatin and nucleus pyknosis were observed, which is a phenomenon of early apoptosis by the emission of bright fluorescence. Appearance of nuclear condensation, nuclear fragmentation and membrane blebbing leading in complex **4** treated cells and change of colour from green into reddish orange fluorescence picturing confirms the apoptotic mode of cell death.

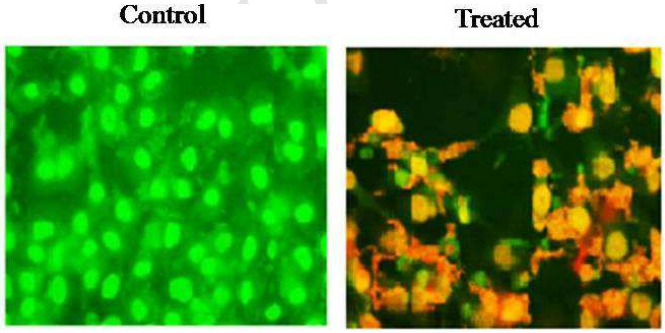

Fig.6. Fluorescent double staining displaying the shift in nuclear morphology.

The tissue selective diagnosis of cell death has been reviewed by incubating the A549 cancer cells with IC_{50} dose of complex **4** for 48 h and then monitoring those gross cytological changes by using Hoechst 33258 staining. The apoptotic characteristics i.e. nuclear shrinkage and chromatin condensation which laid out typical features of cells undergoing apoptosis were observed in Figure 7.

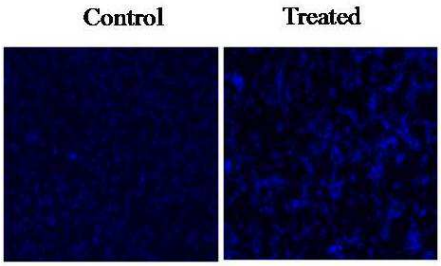

Fig.7. Hoechst 33258 staining of lung adenocarcinoma A549 cells on control and treated with complex **4** at IC_{50} concentrations showing the morphological changes.

3.7. Apoptosis Induction - Flow Cytometry Analysis

To the extent of understanding the mechanism involved in the growth inhibition activity of the complexes, the mechanism of cell death was analysed by flow cytometry method and the portions of cell populations in distinct quadrants are determined by applying quadrant statistics. The mode of cell death was identified by flow cytometric technique using the Annexin V protocol. Inspection is straightforward to implement and differentiates between intact cells ($FITC/PI^-$), apoptotic ($FITC^+/PI^-$) and necrotic cells ($FITC^+/PI^+$). The lung adenocarcinoma A549 cells were incubated with three distinct concentrations (25, 50 and 100 µM) of the complex **4** at 48 h preparation period and the results are shown in Figure 8. The Q2 population (Annexin V^+/PI^+) represented cells withstanding apoptosis with rising from 1.7%, 18.1% and 22.6 % for 25 µM, 50 µM and 100 µM concentrations of investigated arene ruthenium(II) benzhydrazone complex. The results clearly indicate the complex induces apoptosis with different potencies against A549 cells and the observation is in agreement with the *in vitro* MTT assay.

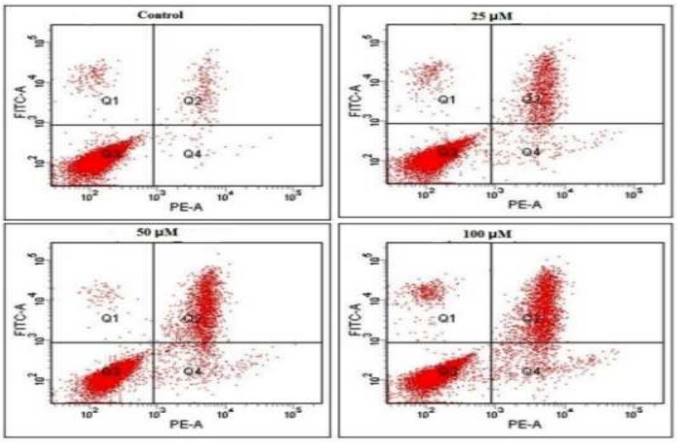

Fig.8. Flow cytometry analysis outcome after the incubation of A549 cells treated with complex **4** at (25-100 µM) for 48 h.

3.8. Cell cycle analysis

Some of the anticancer drugs can motive cell death through obstruction accompanied by cell-cycle mechanism [47], while others follow cell death approach through programmed pathway [48,49]. To examine the response of the complex on the cell cycle capture, A549 cells were incubated with 25 and 50 μM of complex **4** for 24 h treatment. The cell cycle arrest was analysed by using flow cytometry in PI-stained cells. The histograms of DNA distribution in the A549 cells are illustrated in Fig. 9. The percentage in the cells at P3 populations resulting a decrease of 59.7% and 53.5% for complex **4** at 25 & 50 μM concentrations followed by a corresponding reduction of 14.2% and 11.2% in the percentage of cells in G2/M phase. Analysing the FACS histogram statistics, the percentage of apoptotic cells (3.5%) for control considerably increased from 11% to 17.8% after treatment of A549 cells with the complex **4**. Increase in the percentage in the cells at G0/G1 phase shows that the anticancer mechanism stimulated by complex **4** in the A549 cells was a G0/G1 phase arrest. Although the complex **4** displays somewhat changes in cytotoxicity facing A549 cells related with the other complexes, it causes the better apoptotic induction. Hence, the apoptotic effect is depends upon the structure of the complex in addition to cytotoxicity.

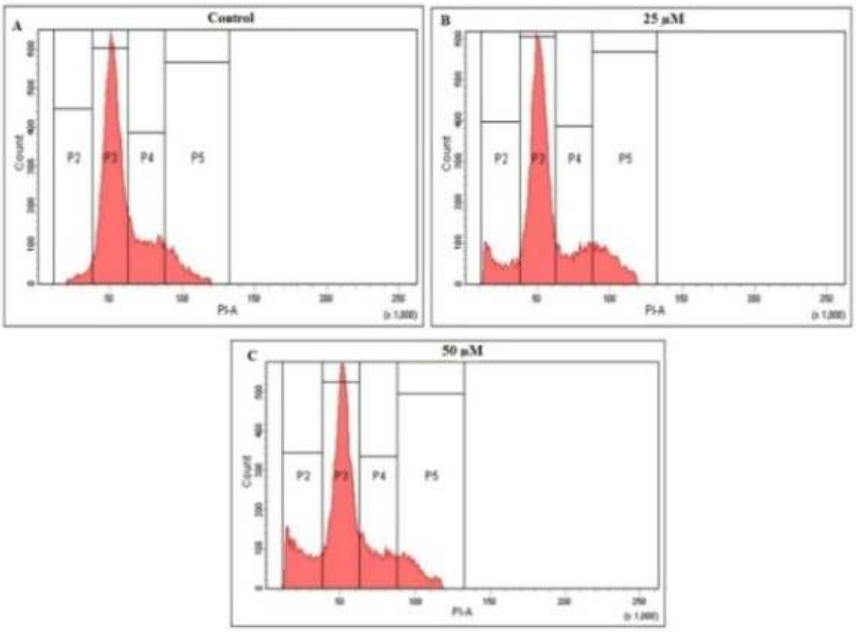

Fig.9. Cell cycles phase distribution of A549 cells (A) control and treated with complex **4** at 25 and 50 μM concentrations (B and C) respectively.

4. Conclusions

A new series of arene ruthenium (II) complexes incorporating flat aromatic pyrene-1-carboxaldehye benzhydrazone ligands have been synthesised and fully characterised by using analytical and various spectral methods. The molecular structures from single crystal X-ray method clearly shows the presence of a pseudo-octahedral ‘‘piano-stool’’ geometry. The differences in biological activity of the organometallic complexes was explained on the basis of partition coefficient values and differences in the energy of ruthenium–chloride bonds i.e. the ability to exchange chlorine ligand into water under cellular conditions. It is worth to note that the cytotoxicity of complex **4** towards A549 cancer cell lines was significantly superior to that of cisplatin. The higher cytotoxicity of the *p*-cymene complexes may be due to the effect of substituent at arene moiety in addition to lipophilic character of heterocyclic pyrene pendant group present in these complexes. Fluorescence dual staining techniques and flow cytometry results shown that the complex **4** promotes apoptosis in A549 cancer cells. Furthermore, cell cycle arrest evidences that the complex **4** inhibit the cell growth at the G0/G1 phase in a dose-dependent manner. The obtained results of the new ruthenium arene benzhydrazone complexes represent the first steps towards forgiving the mechanism of action and the suitable candidates for the development of molecular targeted metal based anticancer agents in order to overcome cisplatin resistance.

Acknowledgements

One of the authors (R.R.K) thanks the DST, Government of India for DST-INSPIRE Senior Research Fellowship (IF130075). We express our genuine thanks to UGC-SAP and DST-FIST for the use of Bruker 400 MHz NMR, UV-visible, Fluorescence and HRMS facilities at the School of Chemistry, Bharathidasan University. Calculations have been carried out using resources provided by Wroclaw Centre for Networking and Supercomputing (http://wcss.pl), grant No 18.

Appendix A. Supplementary data

CCDC 1543439, 1522090, 1522136 and 1517739 contains the supplementary crystallographic data for the ligands and complex. This data can be obtained free of charge from the Cambridge Crystallographic Data Center via www.ccdc.cam.ac.uk/dat_request/cif.

References

[1] B. Rosenberg, L. Vancamp, Nature 222 (1969) 385-386.

[2] W. Han Ang, P. J. Dyson, Eur. J. Inorg.Chem. 2006(2006) 4003-4018.

[3] M. Galanski, M. A. Jakupec, B. K. Keppler, Curr. Med. Chem. 12 (2005) 2075-2094.

[4] S. P. Fricker, Dalton Trans. (2007) DOI: 10.1039/b705551j, 4903-4917.

[5] C. S. Allardyce, P. J. Dyson, Platin. Met. Rev. 45(2001) 62-69.

[6] I. Kostova, Curr. Med. Chem. 13(2006) 1085-1107.

[7] C. G. Hartinger, P. J. Dyson, Chem. Soc. Rev. 38(2009) 391-401.

[8] A. F. Peacock, P. J. Sadler, Chem Asian J. 3(2008) 1890-1899.

[9] P. J. Dyson, CHIMIA Int.J. Chem. 61(2007) 698-703.

[10] S. J. Dougan, P. J. Sadler, CHIMIA Int.J. Chem. 61(2007) 704-715.

[11] G. Suss-Fink, Dalton Trans. 39(2010)1673-1688.

[12] O. Nováková, A. A. Nazarov, C. G. Hartinger, B. K. Keppler, V. Brabec, Biochem Pharmacol.77(2009) 364-374.

[13] H. Chen, J. A. Parkinson, S. Parsons, R. A. Coxall, R. O. Gould, P. J. Sadler, J. Am. Chem. Soc. 124(2002) 3064-3082.

[14] R. Aird, J. Cummings, A. Ritchie, M. Muir, R. Morris, H. Chen, P. Sadler, D. Jodrell, Br. J. Cancer 86(2002) 1652-1657.

[15] C. Scolaro, A. Bergamo, L. Brescacin, R. Delfino, M. Cocchietto, G. Laurenczy, T. J. Geldbach, G. Sava, P. J. Dyson, J. Med. Chem. 448(2005)4161-4171.

[16] A. Weiss, R. H. Berndsen, M. Dubois, C. Müller, R. Schibli, A. W. Griffioen, P. J. Dyson, P. Nowak-Sliwinska, Chem. Sci. 5(2014) 4742-4748.

[17] J. Palmucci, F. Marchetti, R. Pettinari, C. Pettinari, R. Scopelliti, T. Riedel, B. Therrien, A. Galindo, P. J. Dyson, Inorg. Chem. 55 (2016) 11770-11781.

[18] N. Wambang, N. g. Schifano-Faux, A. Martoriati, N. Henry, B. Baldeyrou, C. Bal-Mahieu, T. Bousquet, S. Pellegrini, S. Meignan, K. Cailliau, Organometallics 35(2016) 2868-2872.

[19] K.Nagaraju, S.Pal, J.Organomet.Chem.737 (2013) 7-11.

[20] N. Raja, N. Devika, G. Gupta, V. L. Nayak, A. Kamal, N. Nagesh, B. Therrien, J. Organomet.Chem. 794(2015) 104-114.

[21] R. Pettinari, C. Pettinari, F. Marchetti, C. M. Clavel, R. Scopelliti, P. J. Dyson, Organometallics 32(2012) 309-316.

[22] K. J. Kilpin, P. J. Dyson, Chem. Sci. 4(2013) 1410-1419.

[23] P. K. Singh, D. N. Kumar, Spectrochim. Acta, Part A. 64(2006) 853-858.

[24] B. Singh, R. Srivastava, K. K. Narang, Synth. React. Inorg. Met.-Org.Chem. 30(2000) 1175-1192.

[25] V. Onnis, M. T. Cocco, R. Fadda, C. Congiu, Bioorg. Med. Chem. 17(2009) 6158-6165.

[26] Y. Gou, Y. Zhang, J. Qi, Z. Zhou, F. Yang, H. Liang, J. Inorg. Biochem. 144(2015) 47-55.

[27] P. Sathyadevi, P. Krishnamoorthy, R. R. Butorac, A. H. Cowley, N. S. Bhuvanesh, N. Dharmaraj, Dalton Trans. 40(2011) 9690-9702.

[28] M. M. Đorđević, D. A. Jeremić, M. V. Rodić, V. S. Simić, I. D. Brčeski, V. M. Leovac, Polyhedron 68(2014) 234-240.

[29] D. S. Raja, N. S. Bhuvanesh, K. Natarajan, Dalton Trans. 41(2012) 4365-4377.

[30] M. Alagesan, P. Sathyadevi, P. Krishnamoorthy, N. Bhuvanesh, N. Dharmaraj, Dalton Trans. 43(2014) 15829-15840.

[31] M. A. Bennett, A. K. Smith, J. Chem. Soc. Dalton Trans. (1974) DOI: 10.1039/dt9740000233, 233-241.

[32] O. V. Dolomanov, L. J. Bourhis, R. J. Gildea, J. A. K. Howard, H. Puschmann, J. Appl. Crystallogr. 42 (2009) 339-341.

[33] G. Sheldrick, Acta Crystallogr., Sect. A, 64(2008) 112-122.

[34] R. K. Gupta, R. Pandey, G. Sharma, R. Prasad, B. Koch, S. Srikrishna, P.-Z. Li, Q. Xu, D. S. Pandey, Inorg. Chem. 52(2013) 3687-3698.

[35] K. Morokuma, Chemical Physics Letters 9(1971) 129-132.

[36] T. Ziegler, A. Rauk, Theor. Chem.Acc. 46(1977) 1-10.

[37] R. Tribó, J. Pons, R. Yáñez, J. F. Piniella, Á. Alvarez-Larena, J. Ros, Inorg. Chem.Commun. 3(2000) 545-549.

[38]M.Jahncke,A.Neels,H.Stoeckli-Evans,G.Süss-Fink,J.Organomet.Chem.561(1998) 227-235.

[39] H. Kurosawa, H. Asano, Y. Miyaki, Inorganica Chim. Acta. 270(1998) 87-94.

[40] R. N. Prabhu, R. Ramesh, RSC Adv. 2(2012) 4515-4524.

[41] S. J. Dougan, M. Melchart, A. Habtemariam, S. Parsons, P. J. Sadler, Inorg. Chem. 45(2006) 10882-10894.

[42] R. E. Morris, R. E. Aird, P. del Socorro Murdoch, H. Chen, J. Cummings, N. D. Hughes, S. Parsons, A. Parkin, G. Boyd, D. I. Jodrell, P. J. Sadler, J. Med.Chem. 44(2001) 3616-3621.

[43] P. Ramadevi, R.Singh, S. Jana. R. Devkar, D. Chakraborty, J. Organomet. Chem. 833(2017) 80-87.

[44] I. Ivanovic, K. Javanoic, N. Gligorijevic, S. Radulovic,V.B. Arion, K.S.A.M. Sheweshein, Z.L. Tesic, S.Grguricsipka, J. Organomet. Chem. 794(2014) 343-349.

[45] Y. Chen, M.-Y. Qin, J.-H. Wu, L. Wang, H. Chao, L.-N. Ji , A.-L. Xu, Eur. J. Med. Chem. 70(2013) 120-129.

[46] F. Arnesano, G. Natile, Coord. Chem. Rev. 253(2009) 2070-2081.

[47] V. Dirsch, D. Antlsperger, H. Hentze, A. Vollmar, Leukemia 16(2002) 74.

[48] L. Gamet-Payrastre, P. Li, S. Lumeau, G. Cassar, M.-A. Dupont, S. Chevolleau, N. Gasc, J. Tulliez, F. Tercé, Cancer Res. 60(2000) 1426-1433.

[49] J. Klucar, M. Al-Rubeai, FEBS Lett. 400(1997) 127-130.

Research Highlights:

- A new series of arene Ru(II) complexes containing flat aromatic benzhydrazone ligands have been reported.
- The spectroscopic and structural features of the complexes were studied.
- The *in vitro* cytotoxicity of the complexes on two human cancer cell lines was tested.
- Complex induces cell death *via* apoptosis pathway in cancer cells.
- Cell cycle arrest and apoptosis are responsible for cytotoxicity of these complexes.